Functional Conversion Between A-Type and Delayed Rectifier K^+ Channels by Membrane Lipids

Dominik Oliver *et al.*

Science **304**, 265 (2004);
DOI: 10.1126/science.1094113

Science (print ISSN 0036-8075; online ISSN 1095-9203) is published weekly, except the last week in December, by the American Association for the Advancement of Science, 1200 New York Avenue NW, Washington, DC 20005.

Chemical Change, C. N. Hewitt, W. T. Sturges, Eds. (Elsevier, New York, 1993), pp. 169–231.
5. A. Stohl *et al.*, *J. Geophys. Res.* **108**, 10.1029/2002JD002490 (2003).
6. H. Fischer *et al.*, *Geophys. Res. Lett.* **27**, 97 (2000).
7. P. Hoor, H. Fischer, L. Lange, J. Lelieveld, D. Brunner, *J. Geophys. Res.* **107**, 10.1029/2000JD000289 (2002).
8. A. Zahn *et al.*, *J. Geophys. Res.* **107**, 10.1029/2001JD001529 (2002).
9. J. E. Dibb *et al.*, *J. Geophys. Res.* **108**, 10.1029/2001JD001347 (2003).
10. R. A. Plumb, M. K. W. Ko, *J. Geophys. Res.* **97,** 10145 (1992).
11. R. A. Plumb, D. W. Waugh, M. P. Chipperfield, *J. Geophys. Res.* **105,** 10047 (2000).
12. J. Lelieveld *et al.*, *Geophys. Res. Lett.* **24**, 603 (1997).
13. C. D. Nevison *et al.*, *Global Biogeochem. Cycles* **13**, 737 (1999).
14. D. M. Murphy, D. W. Fahey, *J. Geophys. Res.* **99**, 5325 (1994).
15. C. M. Volk *et al.*, *J. Geophys. Res.* **102**, 25543 (1997).
16. C. A. Ennis, Ed., *Scientific Assessment of Ozone Depletion: 2002* [World Meteorological Organization (WMO), Geneva, 2003].
17. T. E. Graedel, W. C. Keene, *Global Biogeochem. Cycles* **9**, 47 (1995).
18. B. Vierkorn-Rudolph, K. Backmann, B. Schwarz, F. X. Meixner, *J. Atmos. Chem.* **2**, 47 (1984).
19. J. A. Neuman *et al.*, *Rev. Sci. Inst.* **71**, 3886 (2000).
20. J. A. Neuman *et al.*, *Atmos. Environ.* **35**, 5789 (2001).
21. We measured O_3 by a fast-response, dual-beam, ultraviolet-absorption ozone photometer with an overall uncertainty of 5% (*36*). We measured NO_y with an NO/O_3 chemiluminescence instrument (*37*) with an overall uncertainty of ± (0.015 ppbv + 9%); H_2O with a Lyman-α photofragment fluorescence hygrometer (*38*) with an accuracy of ±10%; CO by tunable diode laser absorption with precision of ±7.4 ppbv; and condensation nuclei with a nucleation-mode aerosol size spectrometer (*39*) with a combined uncertainty of ±38%. The tropopause height was measured with a microwave temperature profiler (*40*) within an accuracy of 0.5 km. Temperature and pressure were measured with aircraft probes, with accuracies of 0.5 K and 0.5 hPa, respectively.
22. J. R. Holton *et al.*, *Rev. Geophys.* **33**, 403 (1995).
23. A. F. Tuck *et al.*, *Q. J. R. Meteorol. Soc.* **123**, 1 (1997).
24. K. H. Rosenlof *et al.*, *J. Geophys. Res.* **102**, 13213 (1997).
25. J. M. Russell III *et al.*, *J. Geophys. Res.* **101**, 10151 (1996).
26. C. R. Webster *et al.*, *J. Geophys. Res.* **105**, 11711 (2000).
27. H. A. Michelsen *et al.*, *Geophys. Res. Lett.* **26**, 921 (1999).
28. G. C. Toon *et al.*, *J. Geophys. Res.* **104**, 26779 (1999).
29. A chemical or dynamical definition of the tropopause will give different, usually lower, tropopause heights than the thermal WMO definition (*41*). Here, the primary concern is to identify the stratospheric HCl/O_3 ratio. Because there will often be some tropospheric influence in the LS, choosing the highest commonly accepted tropopause value is the most reliable approach for determining the stratospheric HCl/O_3 ratio. Of the commonly used methods, the thermal tropopause has often been the highest value (*41*).
30. J. A. Logan, *J. Geophys. Res.* **104**, 16115 (1999).
31. The doubling of the IMPACT HCl surface boundary condition to 0.17 ppbv resulted in changes in the UT (pressure altitudes above 220 hPa) of less than 2% for much of the globe, with peak differences of 5 to 10%. The model results give HCl abundances of less than 0.01 ppbv for much of the global UT with either HCl surface value, because of the very low efficiency of transport of surface HCl to the UT and the lack of any local HCl source in the UT.
32. E. C. Richard *et al.*, *J. Geophys. Res.* **108**, 10.1029/2003JD003884 (2003).
33. An estimate of the time before upper troposphere air mixes with lower tropospheric air is given by the turnover time of the tropical upper troposphere of ~10 days (*42*). The times might be longer for regions at higher latitudes away from convection.
34. O. Wild *et al.*, *J. Geophys. Res.* **108**, 10.1029/2002JD003283 (2003).
35. D. A. Hauglustaine, G. P. Brasseur, *J. Geophys. Res.* **106**, 32337 (2001).
36. M. H. Proffitt, R. L. McLaughlin, *Rev. Sci. Instrum.* **54**, 1719 (1983).
37. B. A. Ridley *et al.*, *J. Geophys. Res.* **99,** 25519 (1994).
38. E. M. Weinstock *et al.*, *Rev. Sci. Instrum.* **65**, 3544 (1994).
39. J. C. Wilson, W. T. Lai, S. D. Smith, *J. Geophys. Res.* **96**, 17415 (1991).
40. R. F. Denning, S. L. Guidero, G. S. Parks, B. L. Gary, *J. Geophys. Res.* **94**, 16757 (1989).
41. S. Bethan, G. Vaughan, S. J. Reid, *Q. J. R. Meteorol. Soc.* **122**, 929 (1996).
42. M. J. Prather, D. J. Jacob, *Geophys. Res. Lett.* **24**, 3189 (1997).
43. We thank the pilots and crew of the NASA WB-57F for making the airborne measurements presented here possible, J. C. Wilson for use of condensation nuclei data, and L. L. Gordley and A. Stohl for helpful discussions. Partially supported by NASA's Upper Atmospheric Research Program and Radiation Science Program. Work at the Jet Propulsion Laboratory (R.J.S. and M.J.M.) was carried out under contract with NASA. Participation of LLNL authors occurred through the University of California under the auspices of the U.S. Department of Energy contract no. W-7405-ENG-48.

Supporting Online Material
www.sciencemag.org/cgi/content/full/304/5668/261/DC1
SOM Text
Fig. S1
References and Notes

7 November 2003; accepted 11 March 2004

Functional Conversion Between A-Type and Delayed Rectifier K^+ Channels by Membrane Lipids

Dominik Oliver,[1]* Cheng-Chang Lien,[1]* Malle Soom,[2] Thomas Baukrowitz,[2] Peter Jonas,[1]† Bernd Fakler[1]†

Voltage-gated potassium (Kv) channels control action potential repolarization, interspike membrane potential, and action potential frequency in excitable cells. It is thought that the combinatorial association between distinct α and β subunits determines whether Kv channels function as non-inactivating delayed rectifiers or as rapidly inactivating A-type channels. We show that membrane lipids can convert A-type channels into delayed rectifiers and vice versa. Phosphoinositides remove N-type inactivation from A-type channels by immobilizing the inactivation domains. Conversely, arachidonic acid and its amide anandamide endow delayed rectifiers with rapid voltage-dependent inactivation. The bidirectional control of Kv channel gating by lipids may provide a mechanism for the dynamic regulation of electrical signaling in the nervous system.

The action potential (AP) is the fundamental unit of information in the brain (*1*). Its shape is of critical importance in many forms of neuronal signaling (*2*–*5*). Voltage-gated potassium (Kv) channels shape the AP by controlling its repolarization phase and determine the membrane potential and duration of the interspike interval (*1*). Delayed rectifier Kv channels keep single APs short and permit high-frequency trains of APs (*6*). Rapidly inactivating A-type channels help a cell fire at low frequency (*7*) and promote broadening of APs during repetitive activity (*6*).

It is widely accepted that the functional properties of Kv channels are determined by their α- and β-subunits [Kvα families 1 to 4 (*8*) and Kvβ families 1 to 3 (*9*)]. Most Kvα subunits encode delayed rectifier channels with slow inactivation, whereas only a few exhibit A-type behavior (*8*). Inactivation is generated by two distinct mechanisms. One is the N-type (or ball-and-chain) inactivation, in which an N-terminal protein domain of certain Kvα or Kvβ subunits plugs the open channel pore from the cytoplasmic side (*10*); the other is C-type inactivation, which appears to result from constriction or collapse of the channel's selectivity filter (*11*).

Membrane phospholipids and their metabolites are implicated in regulation of excitability and retrograde modulation at synapses (*12*, *13*). Lipid molecules in plasma membranes regulate the gating of ion channel proteins. The phospholipid phosphatidylinositol-4,5-bisphosphate (PIP_2) modifies the gating of inward rectifier (Kir) K^+ channels (*14*–*16*), KCNQ-type K^+ channels (*17*), voltage-gated Ca^{2+} channels (*18*), and transient receptor potential (TRP) channels (*19*). The polyunsaturated fatty acid arachidonic acid (AA) and its amide anandamide modulate two-pore–domain K^+ channels (*20*) and TRP channels (*21*). Lipid effects on Kv channels, however,

[1]Institute of Physiology, University of Freiburg, Hermann-Herder-Straβe 7, 79104 Freiburg, Germany. [2]Institute of Physiology II, University of Jena, Teichgraben 8, 07744 Jena, Germany.

*These authors contributed equally to this work.
†To whom correspondence should be addressed. E-mail: bernd.fakler@physiologie.uni-freiburg.de (B.F.) and peter.jonas@physiologie.uni-freiburg.de (P.J.)

have remained controversial. Thus, AA accelerates inactivation of A-type channels (*22*, *23*), but has highly variable effects on delayed rectifier K^+ channels (*22*, *24*, *25*), and the effects of PIP_2 and anandamide on Kv channels have not yet been investigated.

Effects of membrane lipids on Kv channel inactivation. To determine the effect of membrane lipids on Kv channels, we used mammalian A-type and delayed rectifier Kv channels expressed in *Xenopus* oocytes and applied PIP_2, AA, and anandamide for defined time intervals to giant inside-out patches (*26*). A 10-s application of 10 μM PIP_2 to the intracellular side of the membrane removed rapid inactivation in all Kv channels with N-type inactivation, independent of whether the ball domain resided in the N terminus of the Kvα subunit (subunits Kv1.4 and Kv3.4) or the Kvβ subunit (Kvβ1.1) (Fig. 1A). The effect was highly selective for ball-and-chain inactivation over other gating processes. Activation of Kv channels was unchanged by PIP_2, as indicated by the similar kinetics and by the similar voltage dependence of activation of the prototypic delayed rectifier Kv1.1. (Voltage for half-maximal activation for Kv1.1 was −45.5 ± 2.1 mV before and −43.2 ± 1.6 mV after a 10-s PIP_2 application; n = 6 patches.) C-type inactivation also appeared to be unaffected, because a PIP_2-resistant component of inactivation was present in Kv1.4 but not in the C-type–deficient mutant Kv1.4(K532V) (*27*) (Fig. 2, A and B, insets). Finally, non-N–non-C–type inactivation of Kv4.3 channels (*28*) persisted even after prolonged PIP_2 applications (Fig. 1A).

Although delayed rectifier Kv channels were unaffected by PIP_2, they were markedly altered by application of both AA and anandamide. AA and anandamide induced rapid and complete inactivation in Kv3.1 channels (Fig. 1B, upper and middle panels). The time course of lipid-induced inactivation was monoexponential with time constants (τ_{inact}) of 1.9 ± 0.8 ms (n = 12 patches) for 3 μM AA and 0.7 ± 0.2 ms (n = 6 patches) for 3 μM anandamide. AA-induced inactivation was concentration-dependent, with a steady-state half-maximal effect (median inhibitory concentration) and Hill coefficient for Kv3.1 of 0.08 ± 0.04 μM and 1.01 ± 0.30 (n = 5 patches), respectively. Inactivation by AA and anandamide was observed in all Kv subtypes tested, but it was highly specific for Kv channels over other types of K^+ channels. Thus, Kv4.3 channels, as well as the delayed rectifier Kv1.1, exhibited rapid inactivation in the presence of AA (τ_{inact} of 2.9 ± 0.9 ms, n = 4 patches, and 30.2 ± 6.4 ms, n = 4 patches, for Kv4.3 and Kv1.1, respectively), whereas the non-inactivating KCNQ2/3 and the voltage- and calcium-dependent BK-type K^+ channels were not affected (Fig. 1B, lower panel). The rapid inactivation induced by AA was also observed in heteromeric Kv1.1 + Kvβ1.1 channels in which N-type inactivation was removed by prior application of PIP_2 (Fig. 1C, n = 5 patches).

Mechanism of phosphoinositide action on N-type inactivation. Previous work on Kir channels has shown that interaction with PIP_2 requires both insertion of the phosphoinositide into the plasma membrane and the negative charge of its inositol ring, endowed with phosphate groups (*14*, *16*). We therefore probed these requirements for the PIP_2-mediated prevention of N-type inactivation in Kv channels. Currents through Kv1.4(K532V), Kv3.4, and Kv1.1 + Kvβ1.1 channels were evoked by 400-ms voltage pulses to 40 mV, and inactivation was quantitated by the relative steady-state current (I_{ss}/I_{max}, where I_{ss} is the steady-state current and I_{max} is the maximum current).

Brief (~10 s) applications of PIP_2 were sufficient to induce a long-lasting inhibition of N-type inactivation that persisted after PIP_2 was removed from the intracellular solution, suggesting that the phosphoinositide was inserted into the membrane (Fig. 2A). The PIP_2 effect could be readily abolished by polylysine (polyK, 25 μg/ml), a polycation that binds tightly to the negatively charged headgroups of phosphoinositides, and the effect of PIP_2 was restored by heparin (100 μg/ml), a polyanion known to remove polyK from the patch (*29*) (Fig. 2B). PolyK accelerated the inactivation compared to control conditions, consistent with charge shielding of endogenous PIP_2 (Fig. 2B, inset, and fig. S1A). The contribution of the negatively charged headgroups for the prevention of N-type inactivation was further investigated by application of phosphoinositides with a variable number of phosphate groups at the inositol ring. Although all negatively

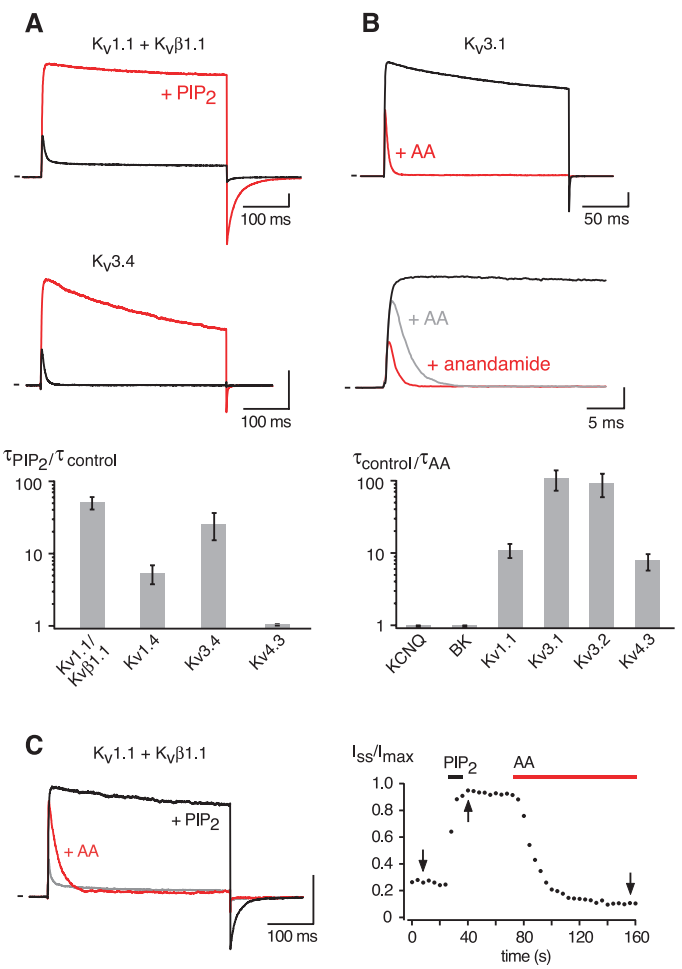

Fig. 1. Bidirectional modification of Kv channel inactivation by lipids. (**A**) Top and middle: Fast N-type inactivation in recombinant A-type channels (Kv1.1 + Kvβ1.1 and Kv3.4) is removed by application of 10 μM PIP_2 to the cytoplasmic side of giant inside-out patches. Currents were recorded in response to voltage pulses from −80 mV to 40 mV before (black) and after (red) a 10-s application of PIP_2; current scale bars are 1 nA. Bottom: PIP_2 selectively affects Kv subtypes with N-type inactivation. Bars representing ratios of the inactivation time constants obtained before and after a 10-s PIP_2 application show mean ± SD of 6 to 14 experiments. (**B**) Top and middle: Rapid inactivation induced in Kv3.1 delayed rectifier channels by 3 μM AA or 3 μM anandamide. Recording conditions are as in (A). Bottom: AA selectively targets Kv channels. Bars representing ratios of the inactivation time constants obtained in the absence and presence of AA show mean ± SD of 9 to 12 experiments. Similar results were obtained with anandamide. (**C**) Left: PIP_2 and AA modify the same Kv channels if applied consecutively. PIP_2 removed fast inactivation of heteromeric Kv1.1 + Kvβ1.1 channels (black), whereas AA (10 μM) reintroduced rapid inactivation (red). Right: Changes in channel inactivation over experimental time. Horizontal bars indicate lipid application, and arrows indicate time points of the traces shown on the left.

charged lipids were equally effective, the uncharged phosphoinositol (PI) failed to prevent inactivation even after extended (for several minutes) applications (Fig. 2C). Similarly, the soluble multivalent anions EDTA (10 mM) and adenosine triphosphate (5 mM) did not affect N-type inactivation ($n = 4$ patches). These results indicated that phosphoinositides inserted into the membrane affect N-type inactivation through electrostatic interactions. These electrostatic interactions were preserved in the presence of the divalent Mg^{2+} at a physiological concentration of 1 mM (Fig. 2D).

The ball-and-chain mechanism of N-type inactivation (*10*) suggests that PIP_2 may exert its effect either by preventing the ball from reaching its receptor or by rendering the receptor insensitive to the ball. To distinguish between these alternatives, the ball-receptor interaction was probed with the synthetic ball-domain peptide from Kv3.4 (*30*) before and after application of PIP_2. The Kv3.4 ball peptide (10 μM) rapidly inactivated Kv1.1 and Kv1.4(K532V) channels both before and after application of PIP_2 (Fig. 3, A and B). These results exclude the possibility that changes in the ball receptor are responsible for preventing N-type inactivation, but suggest that the phosphoinositides may interact with the ball domain itself. Consistent with this hypothesis, PIP_2-containing lipid vesicles specifically bound to the glutathione *S*-transferase (GST)–fused inactivation domains of Kv1.4 and Kv3.4 in a fluorescence-based binding assay (Fig. 3C). Moreover, neutralization of the positive surface-charge cluster observed in the solution structure of the Kv3.4 ball (*31*) (Fig. 3D) considerably reduced the sensitivity of channel inactivation to PIP_2 (Fig. 3D). Thus, a 12-s application of PIP_2 had a rather mild effect on Kv3.4(RK13/14QQ), whereas it largely removed rapid inactivation in wild-type channels (Fig. 3D, inset).

Mechanism of lipid-induced rapid inactivation. Rapid inactivation of ion channels as observed with AA and anandamide on Kv channels may occur by two alternative mechanisms; one is block of the open pore, and the other is induction or modification of a gating process in the channel protein (*32*). We tested these hypotheses by applying AA to the intracellular (inside-out patches) and the extracellular (outside-out patches) sides of the membrane and by probing interference of AA-induced inactivation with the classical open-channel blocker tetraethylammonium (TEA).

AA (4 μM) was equally effective from either side of the membrane ($n = 16$ patches; both patch configurations), and inactivation was reversible upon wash-out of the lipid (Fig. 4A). Independent of the side of application, the onset of AA-induced inactivation was severalfold slower than the solution exchange (time constant ~30 ms). Because channels held in the closed state (at –120 mV) during wash-in of AA exhibited identical inactivation to channels that were repetitively activated until AA-induced inactivation reached a steady state (fig. S2A), this slow time course may reflect partitioning of AA between aqueous solution and lipid membrane rather than use dependence. AA-induced inactivation was not affected by the presence of TEA at the extracellular or intracellular side of the channel protein (Fig. 4B). These results rule out open-channel block as the mechanism underlying AA-induced inactivation, but suggest a lipid-induced gating process.

Although lipid-induced inactivation was unaffected by TEA, it was very sensitive to the ion species permeating the channel (Fig. 5, A and B). Thus, if the outward current evoked by voltage pulses to 60 mV was carried by rubidium (Rb^+), ammonium (NH_4^+), or cesium (Cs^+) instead of K^+, the AA-induced inactivation was substantially reduced (Fig. 5A). In contrast, replacement of K^+ by thallium (Tl^+) did not affect AA-induced inactivation (Fig. 5A). The effects of the various ions correlated with their permeability ratios (P_X/P_K, where P_X is permeability for ion X and P_K is permeability for K^+). The ions with a permeability less than that of K^+ reduced inactivation, whereas Tl^+ with a higher permeability promoted rapid inactivation of Kv3.1 channels (Fig. 5B). The nature of the permeating ion determined the inactivation properties, independent of the side from which it entered the channel and independent of the ions present on the other side of the membrane. Thus, NH_4^+ ions also reduced inactivation when entering the channel from the extracellular side (inward current), whereas K^+ ions permitted rapid inactivation when moving outward even if only NH_4^+ ions were present in the extracellular solution ($n = 5$ patches) (fig. S2B). Although the permeating ion affected the AA-induced inactivation process, AA did

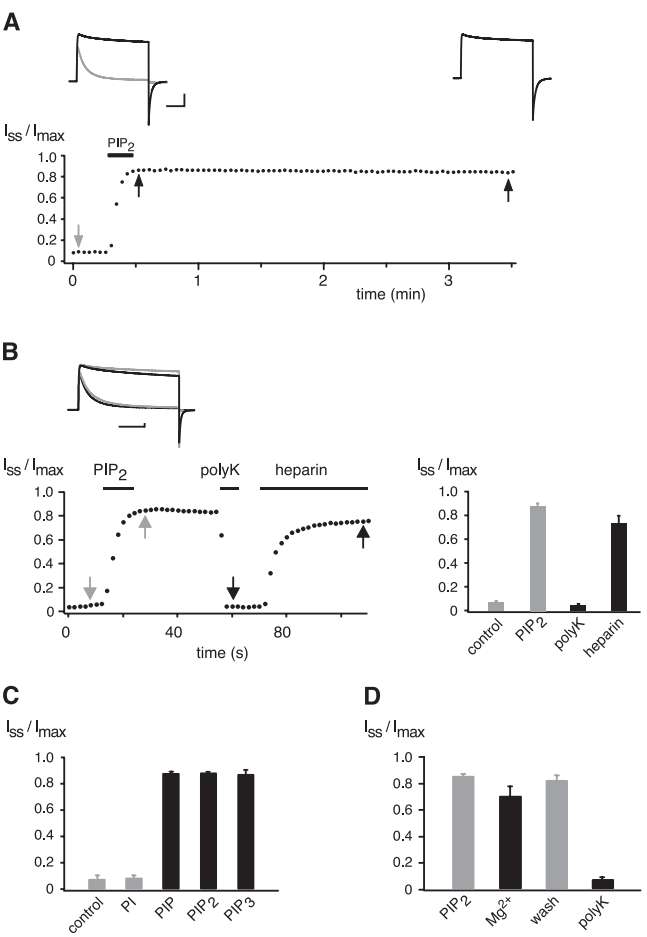

Fig. 2. Prevention of N-type inactivation is mediated by the negatively charged headgroups of membrane-inserted phosphoinositides. (**A**) Removal of N-type inactivation in Kv1.4(K532V) channels induced by short application of PIP_2 (10 μM) persisted for >3 min despite extensive perfusion of the patch. Recording conditions are as in Fig. 1. Insets: Current recordings at the time points indicated by the arrows before and after application of PIP_2. Scale bars, 10 nA and 100 ms. (**B**) Left: Inactivation of Kv1.4(K532V) removed by PIP_2 was restored by polyK (25 μg/μl). Subsequent application of heparin (100 μg/ml) recovered the effect of PIP_2. Inset: Traces recorded at the time points indicated by arrows. Traces before and after PIP_2 are in gray; traces recorded with polyK and heparin are in black. Right: Summary of the effects of PIP_2, polyK, and heparin; data are mean ± SD of eight patches. Similar results were obtained with the Kv1.4 wild type, Kv3.4, and Kv1.1 + Kvβ1.1 channels. (**C**) Phosphatidylinositol-4-phosphate (PIP), PIP_2, and phosphatidylinositol-3,4,5-triphosphate (PIP_3) (10 μM) removed N-type inactivation of Kv1.4(K532V), whereas PI (20 μM) failed to affect inactivation. Data are mean ± SD of five experiments. Similar results were obtained with Kv3.4 and Kv1.1 + Kvβ1.1 channels. (**D**) PIP_2 effects on N-type inactivation of Kv1.4(K532V) channels are preserved in the presence of 1 mM free intracellular Mg^{2+}. Data are mean ± SD of three to five experiments.

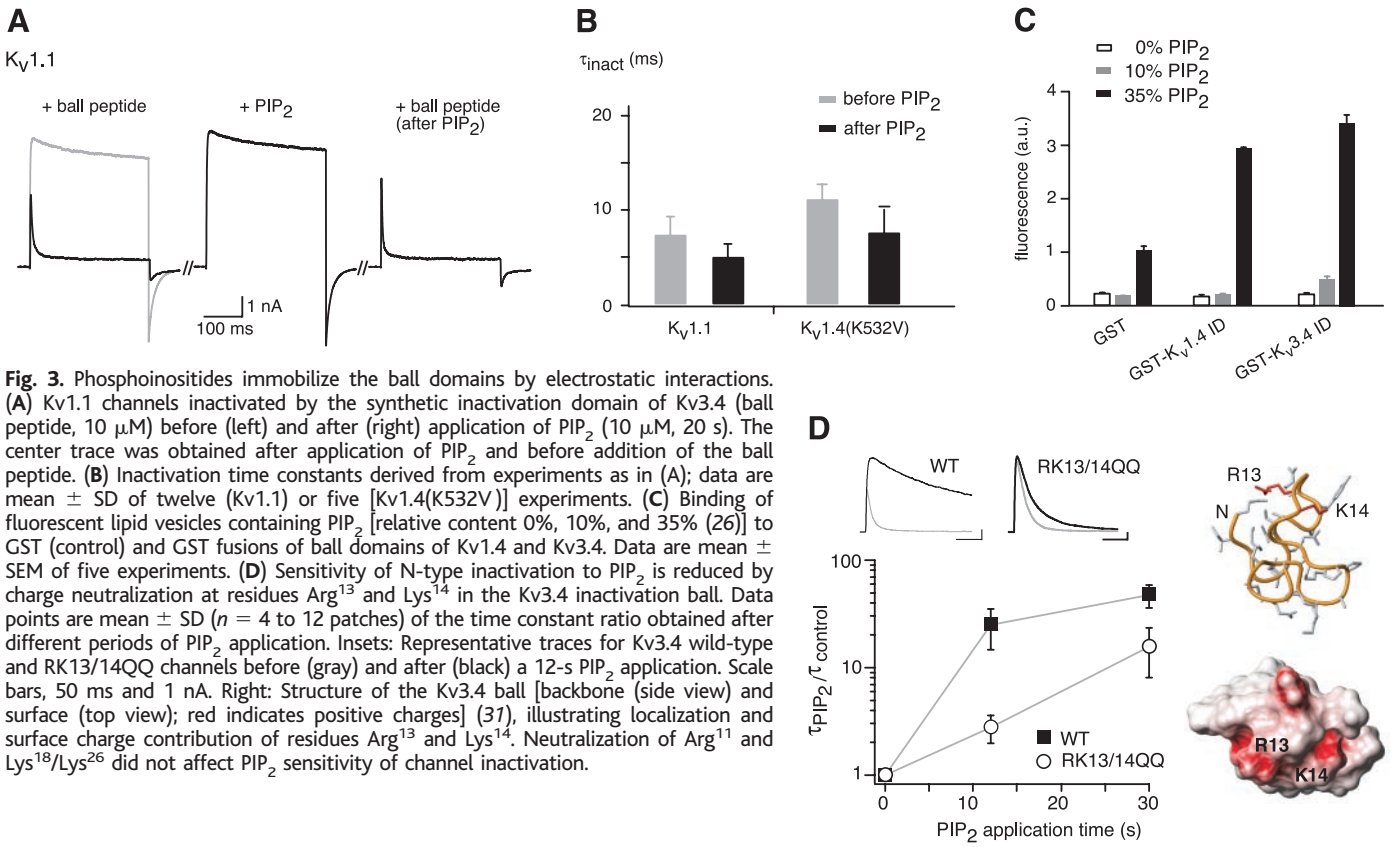

Fig. 3. Phosphoinositides immobilize the ball domains by electrostatic interactions. (**A**) Kv1.1 channels inactivated by the synthetic inactivation domain of Kv3.4 (ball peptide, 10 μM) before (left) and after (right) application of PIP_2 (10 μM, 20 s). The center trace was obtained after application of PIP_2 and before addition of the ball peptide. (**B**) Inactivation time constants derived from experiments as in (A); data are mean ± SD of twelve (Kv1.1) or five [Kv1.4(K532V)] experiments. (**C**) Binding of fluorescent lipid vesicles containing PIP_2 [relative content 0%, 10%, and 35% (*26*)] to GST (control) and GST fusions of ball domains of Kv1.4 and Kv3.4. Data are mean ± SEM of five experiments. (**D**) Sensitivity of N-type inactivation to PIP_2 is reduced by charge neutralization at residues Arg^{13} and Lys^{14} in the Kv3.4 inactivation ball. Data points are mean ± SD (n = 4 to 12 patches) of the time constant ratio obtained after different periods of PIP_2 application. Insets: Representative traces for Kv3.4 wild-type and RK13/14QQ channels before (gray) and after (black) a 12-s PIP_2 application. Scale bars, 50 ms and 1 nA. Right: Structure of the Kv3.4 ball [backbone (side view) and surface (top view); red indicates positive charges] (*31*), illustrating localization and surface charge contribution of residues Arg^{13} and Lys^{14}. Neutralization of Arg^{11} and Lys^{18}/Lys^{26} did not affect PIP_2 sensitivity of channel inactivation.

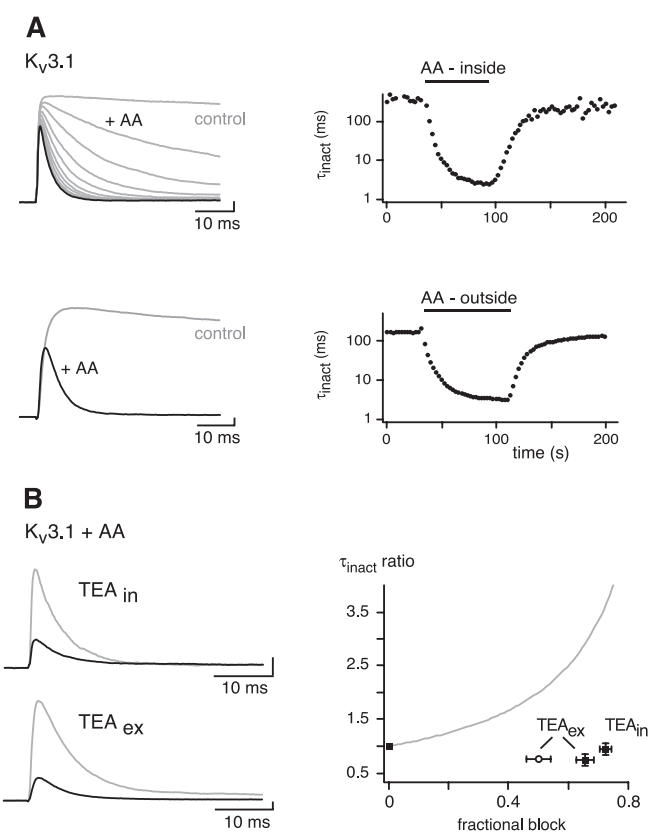

Fig. 4. Lipid-induced inactivation of Kv channels does not involve open-channel block. (**A**) AA induced inactivation in Kv3.1 channels when applied to the cytoplasmic (top) or extracellular (bottom) side of the membrane. Left: Kv3.1 currents (scale bar, 1 nA) before and during AA (4 μM) application; current responses in the upper left panel were recorded at 2-s intervals. Right: τ_{inact} of Kv3.1 current during wash-in and wash-out of AA. (**B**) Left: AA-induced (4 μM) inactivation of Kv3.1 channels (current scale, 1 nA) was unaffected by TEA at the intracellular (30 mM, TEA_{in}) or extracellular (0.3 mM, TEA_{ex}) sides of the channel. Right: τ_{inact} ratio plotted versus the fraction of channels blocked by TEA (closed symbols, n = 5 patches each). The open symbol illustrates the result for Kv3.1(Y407V), in which the high-affinity binding site for extracellular TEA (*41*) had been removed (60 mM TEA, n = 4 patches). The continuous line represents the theoretical relation between changes in τ_{inact} and fractional block of channels, assuming direct competition between TEA and AA (*42*).

not change the permeability of the various cations tested (P_{Rb}/P_K, P_{Cs}/P_K, and P_{NH4}/P_K were 0.81 ± 0.03, 0.16 ± 0.02, and 0.12 ± 0.01, respectively; n = 4 patches).

These results show that lipid-induced inactivation is most likely mediated by a "pore gate" (*32*), whose closure is promoted by AA (through the lipid membrane) and prevented by Cs^+ and NH_4^+ (from the aqueous conduction pathway).

Lipid-induced inactivation regulates the AP phenotype. The transient K^+ currents observed after complete wash-in of AA (Fig. 4A) indicated that lipid-induced inactivation predominantly occurs from the open state, similar to N- and C-type inactivation (*11*). Accordingly, lipid-induced inactivation exhibited strong voltage dependence. Steady-state inactivation of Kv3.1 channels induced by 10 μM AA was adequately described with a Boltzmann function that yielded a potential for half-maximal inactivation of –56.6 ± 1.0 mV and a slope factor of 7.9 ± 0.5 mV (n = 5 patches) (Fig. 5C). Recovery from lipid-induced inactivation was also strongly voltage-dependent, with time constants of 27.0 ± 8.3 ms at –80 mV (n = 8 patches) (Fig. 5D) and 4.0 ± 0.9 ms at –120 mV (n = 3 patches).

Fast onset and slow recovery predict that lipid-induced inactivation changes the neuronal firing pattern through cumulative

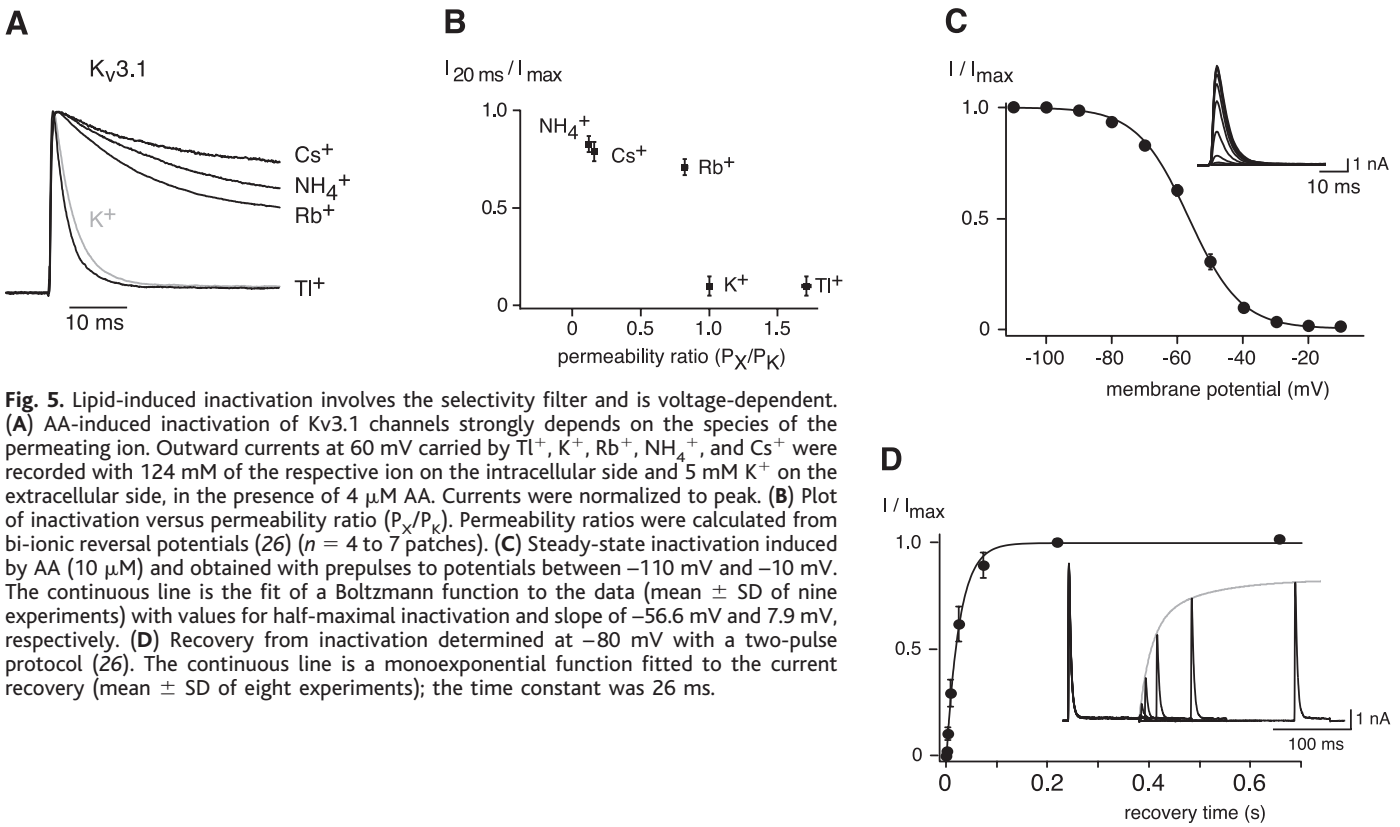

Fig. 5. Lipid-induced inactivation involves the selectivity filter and is voltage-dependent. (**A**) AA-induced inactivation of Kv3.1 channels strongly depends on the species of the permeating ion. Outward currents at 60 mV carried by Tl^+, K^+, Rb^+, NH_4^+, and Cs^+ were recorded with 124 mM of the respective ion on the intracellular side and 5 mM K^+ on the extracellular side, in the presence of 4 μM AA. Currents were normalized to peak. (**B**) Plot of inactivation versus permeability ratio (P_X/P_K). Permeability ratios were calculated from bi-ionic reversal potentials (*26*) (n = 4 to 7 patches). (**C**) Steady-state inactivation induced by AA (10 μM) and obtained with prepulses to potentials between –110 mV and –10 mV. The continuous line is the fit of a Boltzmann function to the data (mean ± SD of nine experiments) with values for half-maximal inactivation and slope of –56.6 mV and 7.9 mV, respectively. (**D**) Recovery from inactivation determined at –80 mV with a two-pulse protocol (*26*). The continuous line is a monoexponential function fitted to the current recovery (mean ± SD of eight experiments); the time constant was 26 ms.

Kv channel inactivation during high-frequency AP trains (*6*, *7*). We have tested this prediction in fast spiking oriens-alveus interneurons that express delayed rectifier K^+ channels mainly assembled from Kv3 subunits (*23*, *33*). In the presence of submicromolar concentrations of AA and anandamide, the Kv currents recorded in nucleated patches displayed pronounced cumulative inactivation (fig. S3A), and the frequency and number of APs elicited by depolarizing current pulses were markedly reduced compared to control conditions (fig. S3B). Thus, lipid-induced inactivation switches a fast-spiking AP phenotype into a slow-adaptive AP pattern.

Discussion. Our results demonstrate that phosphoinositides, the unsaturated fatty acid AA, and anandamide are able to bidirectionally regulate inactivation in recombinant and native Kv channels over a wide range. By preventing N-type inactivation, phosphoinositides can convert A-type channels into delayed rectifiers, while AA and anandamide introduce rapid voltage-dependent inactivation into otherwise non-inactivating channels.

We envisage both lipids to act onto Kv channels by the following distinct molecular mechanisms (fig. S4). PIP_2, through its negatively charged headgroups, immobilizes the positively charged α and β ball domains at the cytoplasmic leaflet of the membrane and thereby prevents them from accessing the pore. In Kv3.4, this electrostatic interaction occurs at the charge cluster formed by Arg^{13} and Lys^{14} at the cap of the ball domain. A similar "trapping the ball" mechanism was proposed for the NIP (N-type inactivation prevention) domain in the Kv1.6 subunit, which neutralizes the activity of the Kv1.4 and Kvβ1.1 inactivation balls when coassembled with these subunits into heteromultimeric channels (*34*). In contrast, AA and anandamide rapidly close Kv channels by inducing conformational alterations in the selectivity filter region that is structurally delineated by the extracellular and intracellular binding sites for TEA (*35*). Thus, the presence of TEA at either site did not interfere with lipid-induced inactivation, whereas the permeant Cs^+, Rb^+, and NH_4^+ ions coordinated in the selectivity filter effectively prevented channel closure. In this context, crystallographic work on the KcsA K^+ channel pore reported two intriguing findings. First, Cs^+ and Rb^+ display a distribution in the selectivity filter that is different from that observed for the smaller K^+ and Tl^+ and that is expected to distinctly affect the dynamics of the filter region (*36*). Second, fatty acids bind to the channel protein close to the selectivity filter and seem to be critical for maintaining the channel in the conducting state (fig. S4) (*37*). Alternatively, the fatty acids may affect stability of the selectivity filter by changing the mechanical properties of the lipid membrane (*38*). The properties of lipid-induced inactivation appear to be unique. Unlike C-type inactivation, it was insensitive to extracellular TEA or to an amino acid exchange at the channel's external vestibule [a homologous site to T449 in *Shaker* (*27*)], and it was insensitive to mutations in the S6 helix reported to affect inactivation in Kv4 channels [a homologous site to V404 and V406 in Kv4.1 (*28*, *39*)].

Our results, together with previous data, strongly suggest that lipid-regulation of Kv channel inactivation is relevant for electrical signaling in the brain. The lipid-Kv channel interaction exhibits high apparent affinity, comparable to that of K_{ATP}-channels for phosphoinositides (*16*) (fig. S1) and of metabolizing enzymes for AA (*40*). Such concentrations of AA and anandamide profoundly change the AP pattern, leading to alterations in both AP shape and frequency (fig. S3), which in turn are expected to affect AP propagation (*2*) and transmitter release from presynaptic terminals (*4*). Consequently, membrane lipids may control the coding properties of neurons and synapses beyond the characteristics set by the expression profile of Kv channel protein subunits.

References and Notes

1. B. Hille, *Ion Channels of Excitable Membranes* (Sinauer, Sunderland, MA, ed. 3, 2001).
2. D. A. Hoffman, J. C. Magee, C. M. Colbert, D. Johnston, *Nature* **387**, 869 (1997).
3. M. Sheng, Y. J. Liao, Y. N. Jan, L. Y. Jan, *Nature* **365**, 72 (1993).

4. J. R. P. Geiger, P. Jonas, *Neuron* **28**, 927 (2000).
5. D. J. Linden, *Neuron* **22**, 661 (1999).
6. C. C. Lien, P. Jonas, *J. Neurosci.* **23**, 2058 (2003).
7. J. A. Connor, C. F. Stevens, *J. Physiol.* **213**, 31 (1971).
8. K. G. Chandy, G. A. Gutman, in *Handbook of Receptors and Channels*, R. A. North, Ed. (CRC Press, Boca Raton, FL, 1995), vol. 2.
9. O. Pongs *et al.*, *Ann. N. Y. Acad. Sci.* **868**, 344 (1999).
10. W. N. Zagotta, T. Hoshi, R. W. Aldrich, *Science* **250**, 568 (1990).
11. G. Yellen, *Q. Rev. Biophys.* **31**, 239 (1998).
12. D. W. Hilgemann, S. Feng, C. Nasuhoglu, *Sci. STKE* **2001**, RE19 (2001).
13. T. F. Freund, I. Katona, D. Piomelli, *Physiol. Rev.* **83**, 1017 (2003).
14. S. L. Shyng, C. G. Nichols, *Science* **282**, 1138 (1998).
15. D. W. Hilgemann, R. Ball, *Science* **273**, 956 (1996).
16. T. Baukrowitz *et al.*, *Science* **282**, 1141 (1998).
17. B. C. Suh, B. Hille, *Neuron* **35**, 507 (2002).
18. L. Wu, C. S. Bauer, X. G. Zhen, C. Xie, J. Yang, *Nature* **419**, 947 (2002).
19. H. H. Chuang *et al.*, *Nature* **411**, 957 (2001).
20. M. Fink *et al.*, *EMBO J.* **17**, 3297 (1998).
21. H. Watanabe *et al.*, *Nature* **424**, 434 (2003).
22. A. Villarroel, T. L. Schwarz, *J. Neurosci.* **16**, 1016 (1996).
23. S. Keros, C. J. McBain, *J. Neurosci.* **17**, 3476 (1997).
24. C. M. Colbert, E. Pan, *J. Neurosci.* **19**, 8163 (1999).
25. E. Honore, J. Barhanin, B. Attali, F. Lesage, M. Lazdunski, *Proc. Natl. Acad. Sci. U.S.A.* **91**, 1937 (1994).
26. Materials and methods are available as supporting material on *Science* Online.
27. J. López-Barneo, T. Hoshi, S. H. Heinemann, R. W. Aldrich, *Recept. Channels* **1**, 61 (1993).
28. H. H. Jerng, M. Shahidullah, M. Covarrubias, *J. Gen. Physiol.* **113**, 641 (1999).
29. T. Krauter, J. P. Ruppersberg, T. Baukrowitz, *Mol. Pharmacol.* **59**, 1086 (2001).
30. C. Antz *et al.*, *Nature Struct. Biol.* **6**, 146 (1999).
31. C. Antz *et al.*, *Nature* **385**, 272 (1997).
32. G. Yellen, *Nature* **419**, 35 (2002).
33. C. C. Lien, M. Martina, J. H. Schultz, H. Ehmke, P. Jonas, *J. Physiol.* **538**, 405 (2002).
34. J. Roeper *et al.*, *Nature* **391**, 390 (1998).
35. D. A. Doyle *et al.*, *Science* **280**, 69 (1998).
36. Y. Zhou, R. MacKinnon, *J. Mol. Biol.* **333**, 965 (2003).
37. F. I. Valiyaveetil, Y. Zhou, R. MacKinnon, *Biochemistry* **41**, 10771 (2002).
38. T. C. Hwang, R. E. Koeppe II, O. S. Andersen, *Biochemistry* **42**, 13646 (2003).
39. D. Oliver, B. Fakler, unpublished data.
40. P. Needleman, J. Turk, B. A. Jakschik, A. R. Morrison, J. B. Lefkowith, *Annu. Rev. Biochem.* **55**, 69 (1986).
41. L. Heginbotham, R. MacKinnon, *Neuron* **8**, 483 (1992).
42. K. L. Choi, R. W. Aldrich, G. Yellen, *Proc. Natl. Acad. Sci. U.S.A.* **88**, 5092 (1991).

43. We thank J. P. Adelman for comments on the manuscript, A. Blomenkamp and S. Eble for technical assistance, H. Kalbacher for the ball peptide, and S. H. Heinemann and R. Klinger for help with the PIP_2-binding assay.

Supporting Online Material
www.sciencemag.org/cgi/content/full/1094113/DC1
Materials and Methods
Figs. S1 to S4
References and Notes

1 December 2003; accepted 19 February 2004
Published online 18 March 2004;
10.1126/science.1094113
Include this information when citing this paper.

REPORTS

Real-Time Quantum Feedback Control of Atomic Spin-Squeezing

JM Geremia,* John K. Stockton, Hideo Mabuchi

Real-time feedback performed during a quantum nondemolition measurement of atomic spin-angular momentum allowed us to influence the quantum statistics of the measurement outcome. We showed that it is possible to harness measurement backaction as a form of actuation in quantum control, and thus we describe a valuable tool for quantum information science. Our feedback-mediated procedure generates spin-squeezing, for which the reduction in quantum uncertainty and resulting atomic entanglement are not conditioned on the measurement outcome.

Quantum systems evolve deterministically when no one is looking. Free from observation, knowledge of a quantum state at one point in time is in principle sufficient to predict its entire evolution. However, when a measurement is performed, quantum mechanics postulates that the observer will obtain a random postmeasurement outcome. Conveniently, measurement can produce states that are difficult to obtain by other means, such as Hamiltonian evolution, and thus provides a powerful tool for quantum state preparation. But standard quantum mechanics does not predict the outcomes of individual experiments, only their likelihood. Measurement-based state preparation is hindered by nondeterminism, and desirable (for example, entangled) quantum states often correspond to highly unlikely measurement outcomes. Here we demonstrate that quantum indeterminism can be reduced by suitable intrameasurement feedback, engineered to steer the outcome of an otherwise random quantum process toward a deterministic outcome.

The quantum system in our experiment was provided by a cloud of N atoms each with intrinsic angular momentum, $\hbar f$, because of a combination of nuclear spin, valence electron spin, and orbital angular momentum. The atoms were initially polarized such that their individual momenta were oriented along a common longitudinal direction, which we chose to be the x axis. The resulting atomic state displayed a net magnetization, $\mathbf{F}$, along x with magnitude $|\mathbf{F}| = \hbar\sqrt{F(F+1)}$, where $F = Nf$. The cartesian components of $\mathbf{F}$ are associated with noncommuting quantum operators, $\hat{F}_x$, $\hat{F}_y$ and $\hat{F}_z$, that obey the Heisenberg uncertainty relation

$$\Delta\hat{F}_y \Delta\hat{F}_z \geq \frac{1}{2}|\langle\hat{F}_x\rangle| \qquad (1)$$

This inequality has the interpretation that an ensemble of measurements (for similarly prepared atomic samples) performed on either $\hat{F}_y$ or $\hat{F}_z$ will yield a distribution of random shot-to-shot outcomes. For a large magnetization, the F_z (for example) measurement distribution is essentially Gaussian with mean $\langle\hat{F}_z\rangle$ and variance $\Delta\hat{F}_z^2 \equiv \langle\hat{F}_z^2\rangle - \langle\hat{F}_z\rangle^2$. The fully polarized atomic state has $\langle\hat{F}_x\rangle = F$ and $\Delta\hat{F}_y = \Delta F_z = \sqrt{F/2}$, and is referred to as a coherent spin state (Fig. 1A)

It is possible to reduce the measurement variance in one of the transverse components below the coherent state value of $F/2$ at the expense of increased uncertainty in the orthogonal component, provided that Eq. 1 remains satisfied (Fig. 1A). Polarized states with this property are referred to as spin-squeezed states (*1*) and have received much attention for their potential to improve the sensitivity of spin-resonance measurements, including magnetometry (*2*, *3*) and atomic clocks (*4*, *5*). Spin-squeezing below the coherent state level is also of fundamental interest in quantum information science for achieving many-particle entanglement (*6*).

Although several different mechanisms have been explored for the preparation of squeezed atomic states (*7*, *8*), interest has focused on using quantum nondemolition (QND) measurements (*9*–*11*), in which the atomic system interacts coherently with an off-resonant optical probe. As a result, the z component of the atomic magnetization, F_z,

Physics and Control and Dynamical Systems, California Institute of Technology, Pasadena, CA 91125, USA.

*To whom correspondence should be addressed. E-mail: jgeremia@caltech.edu